

# Derivation of a Compartmental Model for Quantifying $^{64}\text{Cu}$ -DOTA-RGD Kinetics in Tumor-Bearing Mice

Gregory Z. Ferl<sup>1</sup>, Rebecca A. Dumont<sup>1</sup>, Isabel J. Hildebrandt<sup>1</sup>, Amanda Armijo<sup>1</sup>, Roland Haubner<sup>2</sup>, Gerald Reischl<sup>3</sup>, Helen Su<sup>1</sup>, Wolfgang A. Weber<sup>4</sup>, and Sung-Cheng Huang<sup>1</sup>

<sup>1</sup>Department of Molecular and Medical Pharmacology, David Geffen School of Medicine at UCLA, University of California, Los Angeles, California; <sup>2</sup>Department of Nuclear Medicine, Medical University of Innsbruck, Innsbruck, Austria; <sup>3</sup>Division of Radiopharmacy, University of Tuebingen, Tuebingen, Germany; and <sup>4</sup>Department of Nuclear Medicine, University of Freiburg, Freiburg, Germany

Radiolabeled arginine-glycine-aspartate (RGD) peptides are increasingly used in preclinical and clinical studies to assess the expression and function of the  $\alpha_v\beta_3$  integrin, a cellular adhesion molecule involved in angiogenesis and tumor metastasis formation. To better understand the PET signal obtained with radiolabeled RGD peptides, we have constructed a compartmental model that can describe the time-activity curves in tumors after an intravenous injection. **Methods:** We analyzed 60-min dynamic PET scans obtained with  $^{64}\text{Cu}$ -1,4,7,10-tetraazacyclododecane-*N,N',N'',N'''*-tetraacetic acid (DOTA)-RGD in 20 tumor-bearing severe combined immunodeficient (SCID) mice after a bolus dose (18,500 kBq [500  $\mu\text{Ci}$ ]), using variations of the standard 2-compartment (4k) tissue model augmented with a compartment for irreversible tracer internalization.  $\alpha_v\beta_3$  binding sites were blocked in 5 studies with a coinjection of cold peptide. In addition, 20 h after injection, static PET was performed on 9 of 20 mice. We fitted 2k ( $k_3 = k_4 = 0$ ), 3k ( $k_4 = 0$ ), 4k, and 4k<sub>c</sub> ( $k_4 = \text{constant}$ ) models to the PET data and used several criteria to determine the best model structure for describing  $^{64}\text{Cu}$ -DOTA-RGD kinetics in mice. Akaike information criteria (AIC), calculated from model fits and the ability of each model to predict tumor concentration 20 h after tracer injection, were considered. **Results:** The 4k<sub>c</sub> model has the best profile in terms of AIC values and predictive ability, and a constant  $k_4$  is further supported by Logan-Patlak analysis and results from iterative Bayesian parameter estimation. The internalization compartment allows quantification of the putative tracer internalization rate for each study, which is estimated here to be approximately an order of magnitude less than  $k_3$  and thus does not confound the apparent specific binding of the tracer to the tumor integrin during the first 60 min of the scan. Analysis of specific (S) and nonspecific or nondisplaceable (ND) binding using fitted parameter values showed that the 4k<sub>c</sub> model provided expected results when comparing  $\alpha_v\beta_3$  blocked and nonblocked studies. That is, specific volume of distribution,  $[V_S = (K_1 k_3)/(k_2 k_4)]$ , is much higher

than is nondisplaceable volume of distribution,  $[V_{ND} = (K_1/k_2)]$ , in nonblocking studies ( $2.2 \pm 0.6$  vs.  $0.85 \pm 0.14$ );  $V_S$  and  $V_{ND}$  are about the same in the blocking studies ( $0.46 \pm 1.6$  vs.  $0.56 \pm 0.09$ ). Also, the ratio of static tumor and plasma measurements at 60 and 10 min  $[C_T(60)/C_P(10)]$  is highly correlated ( $R_S = 0.92$ ) to tumor  $V_S$ . **Conclusion:** We have developed and tested a compartmental model for use with the  $^{64}\text{Cu}$ -DOTA-RGD PET tracer and demonstrated its potential as a tool for analysis and design of preclinical and clinical imaging studies.

**Key Words:** compartmental model; pharmacokinetics; small-animal PET; RGD peptide;  $\alpha_v\beta_3$  integrin

**J Nucl Med 2009; 50:250–258**

DOI: 10.2967/jnumed.108.054049

**T**he cell surface glycoprotein  $\alpha_v\beta_3$  is a member of the integrin family whose primary role is mediating interaction between  $\alpha_v\beta_3$ -expressing cells and the extracellular matrix, pathogens, or other cells (1,2).  $\alpha_v\beta_3$  is expressed on certain tumor and endothelial cells and plays an important role in tumor migration and angiogenesis (1,3);  $\alpha_v\beta_3$  antagonists have been shown to induce cell death (1), making this integrin an attractive target for novel cancer therapeutics that inhibit angiogenesis and tumor growth.  $\alpha_v\beta_3$  binds to the arginine-glycine-aspartate (RGD) peptide motif within its *in vivo* protein ligands (e.g., fibrinogen) (2). Small-molecule RGD peptide antagonists with a high affinity for  $\alpha_v\beta_3$  have been developed with the intention of blocking  $\alpha_v\beta_3$  function. Haubner et al. (4) developed the first  $\alpha_v\beta_3$ -specific PET tracer,  $^{18}\text{F}$ -galacto-RGD, and subsequently used it to image patients with cancer (5) in whom a strong association between tracer uptake and  $\alpha_v\beta_3$  expression was observed (6). In squamous cell carcinomas of the head and neck region, uptake of radiolabeled RGD has been suggested to be a potential surrogate parameter of tumor angiogenesis (7). Generally, small-molecule  $\alpha_v\beta_3$  PET tracers are being developed as a means to assess tumor aggressiveness and monitor  $\alpha_v\beta_3$  expression before and after treatment with  $\alpha_v\beta_3$  antagonists.

Received Jun. 2, 2008; revision accepted Nov. 12, 2008.

For correspondence or reprints contact: Gregory Z. Ferl, Department of Molecular and Medical Pharmacology, David Geffen School of Medicine at UCLA, B2-085E CHS, 10833 Le Conte Ave., Los Angeles, CA 90095-6948.

E-mail: gzferl@ucla.edu

Guest Editor: Adriaan A. Lammertsma, VU University Medical Center. COPYRIGHT © 2009 by the Society of Nuclear Medicine, Inc.

To accurately assess the magnitude of specific binding of a PET tracer to  $\alpha_v\beta_3$ , one must be able to separate the PET signal into perfusion and nonspecific and specific binding components. Recently, pharmacokinetic analysis of the  $^{18}\text{F}$ -galacto-RGD PET tracer was performed by Beer et al. (8) using 1- and 2-compartment tissue models fitted to biodistribution data from patients with cancer. Here we applied a similar compartmental modeling approach to the kinetic analysis of the  $^{64}\text{Cu}$ -c(RGDfK(1,4,7,10-tetraazacyclododecane-*N,N',N'',N'''*-tetraacetic acid [DOTA])) ( $^{64}\text{Cu}$ -DOTA-RGD) PET tracer in mouse models bearing tumors grown from cell lines that express low (A431 epidermal carcinoma), intermediate (U373 glioblastoma-astrocytoma), and high (U87 glioblastoma-astrocytoma) levels of  $\alpha_v\beta_3$ . Additionally,  $\alpha_v\beta_3$  binding sites are blocked with a coinjection of cold peptide in selected studies, and 20-h postinjection static PET scans are acquired for selected blocked and nonblocked studies. Four different 2-compartment tissue models are fitted to tumor time–activity curves, and the best model was chosen using the Akaike information criterion (AIC) (9) calculated for each model fitted to both the dynamic scans at 60 min and dynamic data at 20 h after injection. Model-fitting results using a Bayesian or population kinetics approach (10) are also considered. We demonstrated that magnitude of specific binding, as calculated on the basis of fitted model parameters, strongly correlates to the level of  $\alpha_v\beta_3$  expression. The 20-h postinjection scans facilitate estimation of the  $\alpha_v\beta_3$ -mediated tracer internalization rate (11,12) and allow us to determine whether this process confounds measurement of specific binding during the initial 60-min dynamic scan. We also explored the possibility of estimating the capacity of tumor to sequester tracer via specific binding to  $\alpha_v\beta_3$  by deriving a macroparameter equal to the ratio of static tumor and blood-tracer concentration measurements.

## MATERIALS AND METHODS

### c(RGDfK(DOTA)) $^{64}\text{Cu}$ Labeling

The peptide c(RGDfK(DOTA)) was constructed as described previously (13).  $^{64}\text{CuCl}_2$  (specific activity, 185 GBq [5 Ci/mg]) (MDS Norion) was labeled by incubating 1.25  $\mu\text{g}$  of c(RGDfK(DOTA)) with  $^{64}\text{CuCl}_2$  (37 MBq [1 mCi]) for 1 h at 50°C in a total volume of 200  $\mu\text{L}$  of 0.1 M ammonium acetate (pH 7.1). The radiolabeled peptide was purified using a 1-mL strata-X 33- $\mu\text{m}$  polymeric reversed-phase column (Phenomenex, Inc.). After a water wash, the labeled peptide was eluted in 100% ethanol, dried over argon gas at 60°C, and resuspended in 0.9% saline. In vivo metabolic stability of a similar compound,  $^{64}\text{Cu}$ -DOTA-cRGDfK peptide tetramer, was demonstrated by Wu et al. (14), suggesting our monomer has comparable stability.

### Xenograft Model

Severe combined immunodeficient (SCID) mice were purchased from The Jackson Laboratory. All animal manipulations were performed with sterile techniques according to the guidelines of the UCLA Animal Research Committee. U87MG, U373, and A431 cells ( $2 \times 10^6$  cells/mouse) were resuspended in phosphate-buffered saline and Matrigel (BD Biosciences) and injected

subcutaneously into the right front or right rear leg of 7-wk-old male mice. Imaging was performed after tumors had grown to an approximate size of 100  $\text{mm}^3$  as measured using calipers.

### Small-Animal PET and CT

Animals were imaged with a microPET FOCUS 220 scanner (Siemens) and a micro-CAT II scanner (Siemens) (15).  $^{64}\text{Cu}$ -DOTA-RGD (18,500 kBq [500  $\mu\text{Ci}$ ]) was injected via tail vein cannulation. At the time of injection, 60-min dynamic small-animal PET scans with corresponding 7-min micro-CT scans were obtained, followed by 10-min static small-animal PET and micro-CT scans approximately 20 h after injection as previously described (16). For blocked studies, c(RGDfK) (Peptides International) was resuspended in 0.9% saline and mixed with the radiolabeled probe at 10 mg of peptide per kilogram of mouse; scans were acquired as described above. Late-time small-animal PET and micro-CT scans were obtained at approximately 20 h after injection. PET images were reconstructed with filtered backprojection and CT-based attenuation correction. Frame durations were  $20 \times 0.5$  s,  $5 \times 10$  s,  $10 \times 60$  s,  $9 \times 5$  min, and  $1 \times 4$  min for 60-min scans. The 90-min scans used a framing scheme of  $6 \times 10$  s,  $10 \times 60$  s,  $10 \times 5$  min,  $2 \times 10$  min, and  $1 \times 9$  min. A total of 20 mice were used, 4 with both U87 and A431 tumors, for a total of 24 tumor time–activity curves. Here, we primarily considered the results of the 5 blocked and 12 nonblocked studies (17 tumor time–activity curves); 7 additional datasets, collected under slightly different conditions, were used for the population-modeling portion of this study.

### Image Analysis

Using Amide (17), we determined the tracer concentration in tumors by drawing spheric (diameter, 1.5 mm) regions of interest (ROIs) in the area of the reconstructed PET image within the tumor that exhibited the highest radioactivity, as determined by visual inspection. Whole-blood concentration was estimated by drawing an ROI in the region of the image corresponding to the left ventricle of the heart. Activity concentrations are expressed as percentage injected dose per gram of tissue.

### $^{64}\text{Cu}$ -DOTA-RGD Kinetic Model

A linear compartmental model (Fig. 1) was used in this study, where  $u(t)$  represents plasma concentration of the tracer calculated by correcting PET-measured blood concentration for partial-volume effects and absence of uptake by blood cells. A recovery coefficient of 0.7 (18) and hematocrit of 50% (19) are assumed, resulting in a PET-measured whole-blood ( $\text{WB}_{\text{PET}}$ )–to–actual plasma ( $P_a$ ) tracer concentration ratio of

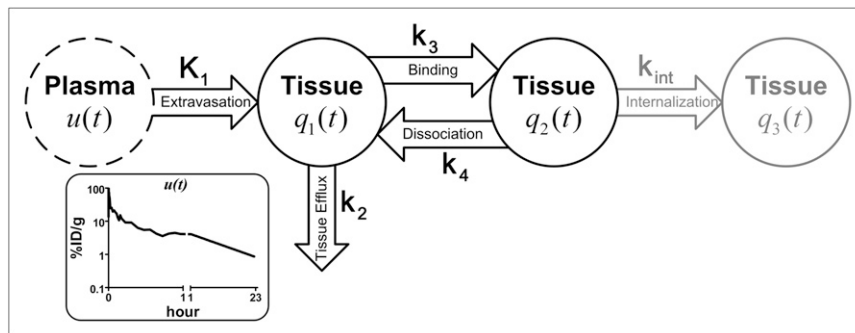
$$\frac{C_{\text{WB}_{\text{PET}}}(t)}{C_{P_a}(t)} \approx 0.7 \times 0.5, \quad \text{Eq. 1}$$

for the 60-min dynamic scans, and

$$\frac{C_{\text{WB}_{\text{PET}}}(t)}{C_{P_a}(t)} \approx 0.5, \quad \text{Eq. 2}$$

for the 20-h postinjection scans, where partial-volume effects are not an issue because of low plasma concentration of tracer and comparable activity in myocardium. Spillover from the myocardium may slightly increase apparent tracer concentration at 20 h

**FIGURE 1.** Compartmental model describing  $^{64}\text{Cu}$ -DOTA-RGD peptide kinetics in tumor.  $u(t)$  represents plasma-forcing function as measured from region corresponding to heart left ventricle in reconstructed PET/CT image, corrected for whole-blood/plasma differences and partial-volume effects (Eqs. 1 and 2). Compartment  $q_1(t)$  represents free or unbound tracer within tumor interstitial space, and compartment  $q_2(t)$  represents tracer bound to  $\alpha_v\beta_3$  integrin. Compartment  $q_3(t)$  represents integrin bound tracer that has been internalized by tumor cell (20) and is assumed to be irreversible.  $K_1$  describes extravasation rate of tracer and has units of  $\text{min}^{-1}$ .  $k_2$  represents tracer flux of free and nonspecifically bound tracer from tissue to plasma and has units of  $\text{min}^{-1}$ .  $k_3$  and  $k_4$  are specific binding and dissociation rates ( $\text{min}^{-1}$ ), and  $k_{\text{int}}$  is tracer internalization rate ( $\text{min}^{-1}$ ). Representative forcing or input function,  $u(t)$ , is shown in inset. %ID/g = percentage injected dose per gram.



after injection; here we assumed spillover error is negligible. Compartments  $q_1(t)$  and  $q_2(t)$  represent the amount of free or nonspecifically bound and specifically bound tracer within tumor extravascular space, respectively. Several model structures could be used to describe the 20-h postinjection data point; here we assumed internalization is a linear process mediated by binding of ligand to receptor, thus, compartment  $q_3(t)$  was added to represent tracer that has been irreversibly internalized by tumor cells (20). Model equations are written as

$$\frac{dq_1(t)}{dt} = K_1 u(t) - (k_2 + k_3)q_1(t) + k_4 q_2(t) \quad \text{Eq. 3}$$

and

$$\frac{dq_2(t)}{dt} = k_3 q_1(t) - (k_4 + k_{\text{int}})q_2(t) \quad \text{Eq. 4}$$

and

$$\frac{dq_3(t)}{dt} = k_{\text{int}} q_2(t), \quad \text{Eq. 5}$$

where, putatively,  $K_1$  represents the tracer extravasation rate ( $\text{min}^{-1}$ ),  $k_2$  represents the rate of tissue efflux of free or nonspecifically bound tracer ( $\text{min}^{-1}$ ), and  $k_3$  represents the rate of specific binding ( $\text{min}^{-1}$ ) of  $^{64}\text{Cu}$ -DOTA-RGD to the extracellular portion of the  $\alpha_v\beta_3$  integrin.  $k_4$  and  $k_{\text{int}}$  represent rates of dissociation ( $\text{min}^{-1}$ ) and internalization ( $\text{min}^{-1}$ ) of specifically bound tracer, respectively. Note that  $k_{\text{int}}$  is assumed to represent internalization; however, all slow uptake mechanisms are lumped into this parameter. The measurement model is written as

$$c(t) = V_B \times u(t) + q_1(t) + q_2(t) + q_3(t), \quad \text{Eq. 6}$$

where  $V_B$  is the fractional blood volume of the tumor (unitless) and  $c(t)$  is the tumor time-activity curve. Here we considered 4 structural perturbations of the model shown in Figure 1: a 2k model ( $k_3 = k_4 = 0$ ) assumes PET data can be accurately described without explicitly accounting for the specific binding of  $^{64}\text{Cu}$ -DOTA-RGD to the  $\alpha_v\beta_3$  integrin; a 3k model ( $k_4 = 0$ ) explicitly accounts for the specific binding of the tracer to integrin, which is assumed to be irreversible; a 4k model assumes reversible

binding of tracer to integrin; and a  $4k_c$  ( $k_4 = \text{constant}; k_4 > 0$ ) model assumes that  $k_4$  has approximately the same value across all datasets. Each of the 4 model variants is augmented with a compartment representing irreversible internalization of tracer by tumor cells (Eq. 5).

### Parameter Estimation

The SAAM II/PopKinetics tracer kinetic modeling program (21,22) was used to implement the model shown in Figure 1 and estimate unknown parameters ( $K_1, k_2, k_3, k_4$ , and  $k_{\text{int}}$ ). Each measured PET data point,  $i$ , was assigned a weight ( $w_i$ ) equal to the reciprocal of the data variance, calculated as follows:

$$w_i = \frac{1}{\sigma_i^2} = \frac{d_i}{\mu_i}, \quad \text{Eq. 7}$$

where  $\sigma_i$  is the SD,  $d_i$  is frame duration, and  $\mu_i$  is mean ROI value. Standard 2-stage (STS) and iterative 2-stage (ITS) parameter-estimation algorithms (10) were implemented using PopKinetics. The STS method sequentially fits a particular model (e.g.,  $4k_c$ ) individually to  $n$  PET-derived datasets using the SAAM II computational engine and calculates the mean and SD of each parameter across all datasets. The ITS method repeats this process using mean and SD values calculated using the STS method as Bayesian constraints (18,23) on the parameter space, resulting in a new set of parameter means and SDs to be used as Bayesian constraints for the next round of fits. This iterative process continues until all parameters reach a preset convergence value. Given a large enough population size,  $n$ , the ITS method can detect fixed effects in the model structure, which occur when the SD of a parameter across all  $n$  datasets approaches zero. All models were fitted to 60-min dynamic scans and then extrapolated to the 20-h postinjection data by extending the simulation time for each fitted model; the input function was extrapolated to 20 h by fitting a single exponential term ( $Ae^{-\lambda t}$ ) to the 60-min and 20-h data points. Additionally, each model was fitted to the 60-min dynamic data plus the 20-h data.

### Model Discrimination

The AIC was used to determine which of the 4 proposed model structures was most appropriate for use with  $^{64}\text{Cu}$ -DOTA-RGD. The AIC (9) considers goodness of fit and structural parsimony with the purpose of selecting a single model, from a group of

candidate models, that best describes the data of interest while not being overly complex. The AIC is written here as

$$\text{AIC} = \frac{1}{2}(\text{J}(\mathbf{p}) + \ln(2\pi)) + \frac{n_{\text{P}}}{n_{\text{D}}}, \quad \text{Eq. 8}$$

and

$$\text{J}(\mathbf{p}) = \frac{1}{n_{\text{D}}} \sum_{i=1}^{n_{\text{D}}} \left( \ln \left( \frac{\mu_i}{d_i} \right) + \frac{(\mu_i - s(\hat{\mathbf{p}}, t_i))^2}{\mu_i/d_i} \right), \quad \text{Eq. 9}$$

where  $\text{J}(\mathbf{p})$  is the objective function used to assess goodness of fit,  $n_{\text{P}}$  is the number of adjustable model parameters,  $n_{\text{D}}$  is the number of data points to which the model is fitted,  $\mathbf{p}$  is the parameter vector that minimizes the objective function, and  $s(\hat{\mathbf{p}}, t_i)$  is the model simulation at time  $t_i$  and parameter vector  $\hat{\mathbf{p}}$  (22). On the basis of this criterion, the model with the lowest calculated AIC value is considered to have achieved the optimal balance between goodness of fit and structural parsimony. Additionally, we considered the ability of each model to predict the 20-h postinjection data by extrapolating models fitted to the initial dynamic PET scan.

### Calculation of Volumes of Distribution

Specific (S) and nondisplaceable (ND), that is, nonspecific, volumes of distribution (V) were calculated for blocked ( $n = 5$ ) and nonblocked ( $n = 12$ ) tracer studies using the following equations (24):

$$V_{\text{S}} = \frac{K_1 k_3}{k_2 k_4}, \quad \text{Eq. 10}$$

and

$$V_{\text{ND}} = \frac{K_1}{k_2}, \quad \text{Eq. 11}$$

where  $K_1$ ,  $k_2$ ,  $k_3$ , and  $k_4$  were calculated by setting  $k_{\text{int}}$  to zero and fitting the model to data from the 60-min dynamic PET scans. Total volume of distribution ( $V_{\text{d}}$ ) is defined as

$$V_{\text{d}} = V_{\text{S}} + V_{\text{ND}} = \frac{K_1}{k_2} \left( 1 + \frac{k_3}{k_4} \right). \quad \text{Eq. 12}$$

Equations 10 and 12 are used only when  $k_4$  is nonzero; Patlak uptake [ $K_i = (K_1 k_3)/(k_2 + k_3)$ ] (25) could be calculated in the case where  $k_4$  is zero.

### Statistical Analysis

All statistical analysis (standard and paired  $t$  test, Spearman correlation, linear regression) was performed using GraphPad Prism (version 4.03 for Windows; GraphPad Software) (available at: <http://www.graphpad.com>).

## RESULTS

### Model Fits to 60-Min Dynamic Scans

Figure 2 shows 2k, 3k, 4k, and  $4k_{\text{c}}$  models fitted to tumor time-activity curves from 4 selected 60-min dynamic scans;  $k_{\text{int}}$  (Eq. 5) is fixed at zero. Qualitatively, the first

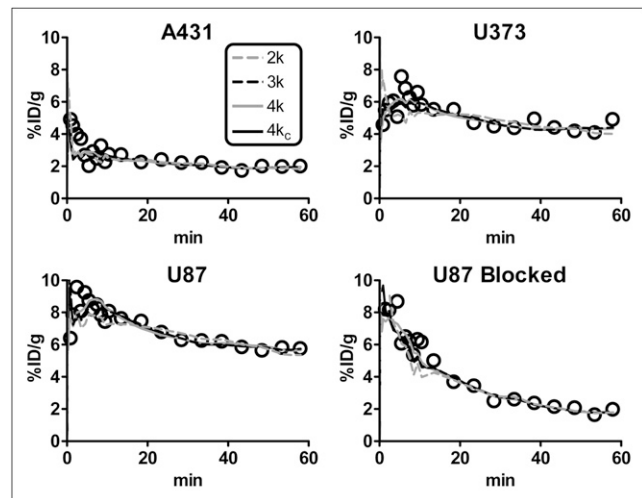


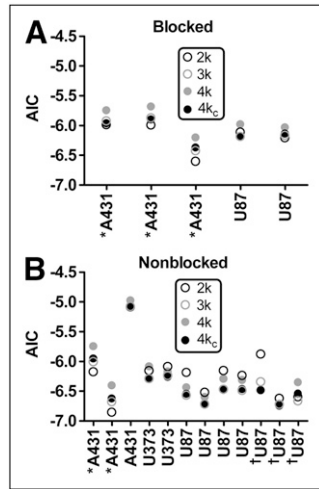
**FIGURE 2.** Representative model fits to data from 60-min dynamic PET scans of mice bearing subcutaneous tumors expressing low (A431), intermediate (U373), or high (U87) levels of  $\alpha_{\text{v}}\beta_3$ . Lower-right-hand panel shows representative model fit to data from mouse that received a coinjection of cold peptide (10 mg/kg) with hot tracer dose. Lines represent 2k, 3k, 4k, and  $4k_{\text{c}}$  models fitted to tumor time-activity curves from 4 selected 60-min dynamic scans (open circles). %ID/g = percentage injected dose per gram.

10 min of some fits are slightly off, possibly because of lower weights assigned to these data points. The mean and SD of the 5 estimated model parameters calculated using STS and ITS estimation methods are  $V_{\text{B}} = 0.049 \pm 0.024$  (unitless) (STS) and  $0.074 \pm 0.044$  (ITS);  $K_1 = 0.046 \pm 0.017 \text{ min}^{-1}$  and  $0.031 \pm 0.011 \text{ min}^{-1}$ ;  $k_2 = 0.18 \pm 0.20 \text{ min}^{-1}$  and  $0.13 \pm 0.12 \text{ min}^{-1}$ ;  $k_3 = 0.041 \pm 0.035 \text{ min}^{-1}$  and  $0.063 \pm 0.029 \text{ min}^{-1}$ ; and  $k_4 = 0.013 \pm 0.006 \text{ min}^{-1}$  and  $0.0094 \pm 0.0 \text{ min}^{-1}$ . These were calculated by applying STS and ITS parameter-estimation methods to the 4k model, which was fitted to all 24 tumor time-activity curves. The ITS method converges to the  $4k_{\text{c}}$  model ( $k_4 = 0.00938 \text{ min}^{-1}$  for all studies) after 23 iterations, using a convergence criterion of 0.05; this value of  $k_4$  was used for the aforementioned  $4k_{\text{c}}$  model fits (Fig. 2) and all subsequent  $4k_{\text{c}}$  fits.

### AIC Analysis of Models Fitted to 60-Min Dynamic Scans

Figure 3A plots AIC values for the blocked  $\alpha_{\text{v}}\beta_3$  studies, in which the 2k model has the lowest value for 4 of 5 fits; Figure 3B shows that the 2k model also has the lowest AIC for 2 of 3 nonblocked A431 studies. 3k and  $4k_{\text{c}}$  models have the lowest values ( $<1\%$  difference between  $\text{AIC}_{3\text{k}}$  and  $\text{AIC}_{4\text{k}_{\text{c}}}$  for each study) for 2 of 2 U373 studies and 5 of 7 U87 studies (Fig. 3B). The 4k model has the highest AIC value for all blocked and A431 studies, and the 2k model has the highest AIC value for 7 of 9 U373 and U87 nonblocked studies. A lower AIC value indicates a more appropriate model structure.

**FIGURE 3.** AIC (Eq. 8) calculated for 2k, 3k, 4k, and 4k<sub>c</sub> models fitted to data from blocked (A) and nonblocked (B) dynamic PET studies. Lower AIC value indicates better fit of model to data. All tumors are located in mouse shoulder, and each PET scan is 60 min unless noted otherwise. \*Tumor located in thigh of mouse. †90-min PET scan.



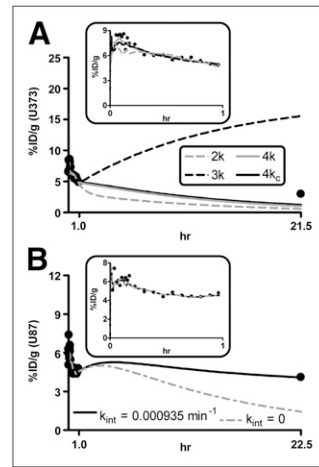
### Extrapolation of Model Fitted to 60-Min Dynamic Data to 20-H Postinjection Data

Figure 4A depicts a representative extrapolation to the 20-h postinjection data using the aforementioned fits to the 60-min dynamic scans. 2k, 4k, and 4k<sub>c</sub> models provide similar extrapolations, with 4k<sub>c</sub> giving a slightly better qualitative prediction; the 3k model predicts a constant accumulation of tracer in tumor, resulting in a much higher predicted concentration than that measured by the 20-h postinjection scan.

### Model Fits to 60-Min Dynamic Data and 20-H Postinjection Data

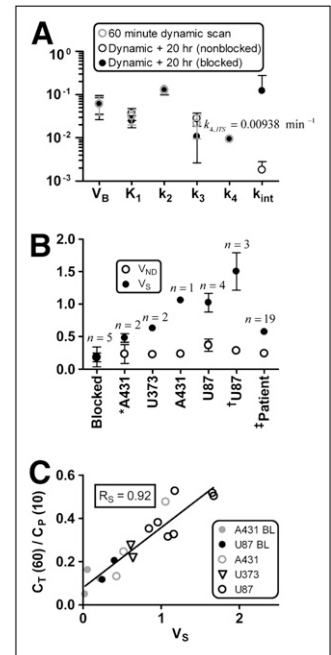
Because the 2k and 4k models performed poorly and the 3k and 4k<sub>c</sub> models performed equally well with respect to AIC analysis (Fig. 3), 3k and 4k<sub>c</sub> models were fitted to data

**FIGURE 4.** Analysis of 20-h postinjection static PET scans. (A) Representative example of prediction of 20-h tracer concentration in tumor based on model fitted to 60-min dynamic scan data from blocked and nonblocked studies; that is, each model was fitted to dynamic scan data (inset) and extrapolated from  $t = 60$  min to the 20-h data point for 2k, 3k, 4k, and 4k<sub>c</sub> models. (B) Representative example of 4k<sub>c</sub> model fitted to data from both 60-min dynamic and 20-h postinjection blocked and nonblocked PET scans (black curve); broken gray curve illustrates effect on simulation of setting estimated internalization rate ( $k_{int}$ ) to zero. Inset more clearly illustrates effect of  $k_{int}$  on first 60 min after tracer injection. %ID/g = percentage injected dose per gram.



from each 60-min dynamic scan plus the 20-h postinjection datum, with  $k_{int}$  (Eq. 5) set as an adjustable parameter. AICs calculated for each fit (not shown) show that 4k<sub>c</sub> has the lower value across the 13 tumor models when fitted to dynamic plus 20-h postinjection scans and, thus, the better structure. Figure 4B depicts a representative fit (black curve) of the 4k<sub>c</sub> model to dynamic PET data plus the 20-h postinjection data with the first hour of data and fit shown in the inset.  $k_{int}$  was then set to zero (gray curve) for the fitted model depicted in Figure 4B; qualitatively, little change is seen during the first hour of the simulation (Fig. 4B, inset), whereas a dramatic decrease in tumor concentration is seen over the remaining 17 h of the simulation (Fig. 4B). Figure 5A compares estimated values of  $V_B$ ,  $K_1$ ,  $k_2$ , and  $k_3$  based on the 4k<sub>c</sub> model fitted to 60-min dynamic data only and 60-min dynamic data plus the 20-h postinjection data (nonblocked and blocked studies). Estimated values of  $V_B$ ,  $K_1$ ,  $k_2$ , and  $k_3$  based on the 4k<sub>c</sub> model fitted to each of these 3 datasets are all similar ( $P > 0.2$ , paired  $t$  test), with the exception of  $k_3$  based on blocked studies with 20-h data (solid black circle,  $P < 0.05$ , paired  $t$  test), which is lower than the other 2 estimated  $k_3$  values (open circles). We compared mean values across all 13

**FIGURE 5.** Results based on 4k<sub>c</sub> model of <sup>64</sup>Cu-DO-TA-RGD kinetics. (A) 4k<sub>c</sub> model fits to dynamic scan data with and without 20-h postinjection data. Comparison of estimated parameters (mean  $\pm$  SD) calculated by fitting model to 60-min dynamic scan data only (open gray circles) and model fitted to both 60-min dynamic scan data and 20-h postinjection data ( $k_{int}$  adjustable), in which fits to blocked (black circles) and nonblocked (open black circles) data are shown.  $k_4$  is fixed to 0.00938 min<sup>-1</sup> for all model fits. (B) Comparison of volumes of distribution (Eqs. 10 and 11) calculated for blocked (A431 and U87 tumors) and nonblocked (A431, U373, and U87 tumors) studies. All tumors were located in mouse shoulder, and each PET scan was 60 min unless noted otherwise. (C) Spearman correlation ( $R_S$ ) between ratio of tracer concentration in tumor at 60 min after injection ( $[C_T(60)]$ ) to tracer concentration in plasma at 10 min ( $[C_P(10)]$ ) and specific volume of distribution ( $V_S$ ). Units for  $K_1$ ,  $k_2$ ,  $k_3$ ,  $k_4$ , and  $k_{int}$  are min<sup>-1</sup>;  $V_{ND}$ ,  $V_S$ , and  $V_B$  are unitless. \*Tumor located in thigh of mouse. †90-min PET scan. ‡Results of 4k model ( $k_{int} = 0$ ) fitted to dynamic <sup>18</sup>F-galacto-RGD peptide PET scans from 19 patients with cancer (8).



tumors with 20-h scans and determined that  $k_{int}$  is approximately an order of magnitude lower than  $k_3$  (Fig. 5A); also, the mean estimated value of  $k_{int}$  based on blocked studies is higher than  $k_{int}$  based on nonblocked studies. Table 1 lists estimated parameter values for the  $4k_c$  model fitted to data from  $\alpha_v\beta_3$  blocked and nonblocked dynamic scans and the 20-h postinjection scan where available; models are fitted to dynamic scan data only, with  $k_{int}$  fixed at zero, for the 4 studies without a delayed static scan.

### Volumes of Distribution

Specific ( $V_S$ ) and nondisplaceable ( $V_{ND}$ ) volumes of distribution (Eqs. 10 and 11) were calculated for all blocked and nonblocked studies using parameter values based on model fits to the 60-min dynamic scans (Table 1). Figure 5B plots mean  $\pm$  SD of both  $V_S$  and  $V_{ND}$  for all blocked and nonblocked studies, with nonblocked organized by tumor type, location, and scan duration. No statistically significant difference between  $V_S$  and  $V_{ND}$  is detected for the blocked studies, and a significant increase in  $V_S$  is observed for the nonblocked studies ( $P < 0.001$ ,  $n = 12$ ), using a standard  $t$  test. Qualitatively, A431 tumors located in the thigh show a small increase in  $V_S$ , whereas all remaining tumor types exhibit a much larger increase. This analysis was repeated using ROIs drawn on regions of the reconstructed PET image corresponding to muscle and liver (not shown). Blocking of  $\alpha_v\beta_3$  via coinjection of cold peptide appeared to have no effect on the relationship between  $V_S$  and  $V_{ND}$  in these

tissues, suggesting that tracer uptake in muscle and liver is independent of  $\alpha_v\beta_3$ .

Additionally,  $V_S$  and  $V_{ND}$  were calculated using values of  $K_1$ ,  $k_2$ ,  $k_3$ , and  $k_4$  estimated by Beer et al. (8) on the basis of dynamic PET scans of 19 patients with cancer; the mean value (shown without SD) across all patients is plotted in Figure 5B. We compared means and found that both  $V_S$  and  $V_{ND}$  calculated from patient PET scans were qualitatively similar to volumes of distribution calculated from our mouse studies ( $[0.635 (n = 19)$  vs.  $0.754 (n = 17)]$  for  $V_S$  and  $[0.271 (n = 19)$  vs.  $0.261 (n = 17)]$  for  $V_{ND}$ ). To obtain parameter values comparable to those listed here, we multiplied each  $K_1$  listed in Beer et al. by 0.45 (patient hematocrit  $\approx 45\%$ ) (26) because tracer concentration in whole blood was used as an input function in the patient study.

Figure 5C depicts the strong correlation ( $R_S = 0.92$ ) that was observed between  $V_S$  and the ratio of tracer concentration in tumor at 60 min after injection [ $C_T(60)$ ] to tracer concentration in plasma at 10 min after injection [ $C_P(10)$ ].

### DISCUSSION

The results of our study suggest that the  $4k_c$  model, derived using the ITS parameter-estimation method, is most appropriate for describing  $^{64}\text{Cu}$ -DOTA-RGD PET data. Figure 6 summarizes the model discrimination process that was applied to the 2k, 3k, 4k, and  $4k_c$  structures. We were able

**TABLE 1.** Estimated Parameter Values for  $4k_c$  Model

Study	Parameter						
	$V_B$	$K_1$	$k_2$	$k_3$	$V_{ND}$	$V_S$	$k_{int}$
<b>Blocked</b>							
A431*	0.0736	0.0323	0.1190	0.0023	0.271	0.066	0.09910
A431*	0.0408	0.0228	0.1370	0.0029	0.166	0.051	0.12700
A431*	0.0539	0.0127	0.1250	0.0202	0.102	0.219	0.00047
U87	0.0236	0.0298	0.1290	0.0164	0.231	0.404	0.00215
U87	0.1140	0.0264	0.1690	0.0115	0.156	0.192	0.38100
<b>Nonblocked</b>							
A431*	0.0478	0.0291	0.0846	0.0139	0.344	0.510	0.00329
A431*	0.0467	0.0159	0.1190	0.0302	0.134	0.430	0.00163
A431	0.0599	0.0291	0.1230	0.0425	0.237	1.072	0.00112
U373	0.0530	0.0341	0.1356	0.0228	0.251	0.612	–
U373	0.0701	0.0346	0.1660	0.0286	0.208	0.636	0.00095
U87	0.0546	0.0518	0.1340	0.0203	0.387	0.837	0.00313
U87	0.0860	0.0407	0.1520	0.0382	0.268	1.090	0.00094
U87	0.0174	0.0452	0.1330	0.0263	0.340	0.953	0.00245
U87	0.0956	0.0451	0.0929	0.0227	0.485	1.175	0.00092
U87†	0.0238	0.0502	0.1640	0.0357	0.306	1.166	–
U87†	0.1212	0.0331	0.1329	0.0626	0.249	1.661	–
U87†	0.1396	0.0330	0.1078	0.0514	0.307	1.678	–

\* Tumor located in thigh of mouse.

† 90-min dynamic PET scan.

Mean percent coefficient of variation for all 68 estimated parameters is  $25\% \pm 20\%$ . All tumors were located in mouse shoulder, and each dynamic PET scan was 60 min unless otherwise noted. Listed values correspond to open and closed black circles in Figure 5A; 4 studies without  $k_{int}$  values correspond to gray circles in Figure 5A. Units for  $K_1$ ,  $k_2$ ,  $k_3$ , and  $k_{int}$  are  $\text{min}^{-1}$ ;  $V_{ND}$ ,  $V_S$ , and  $V_B$  are unitless.

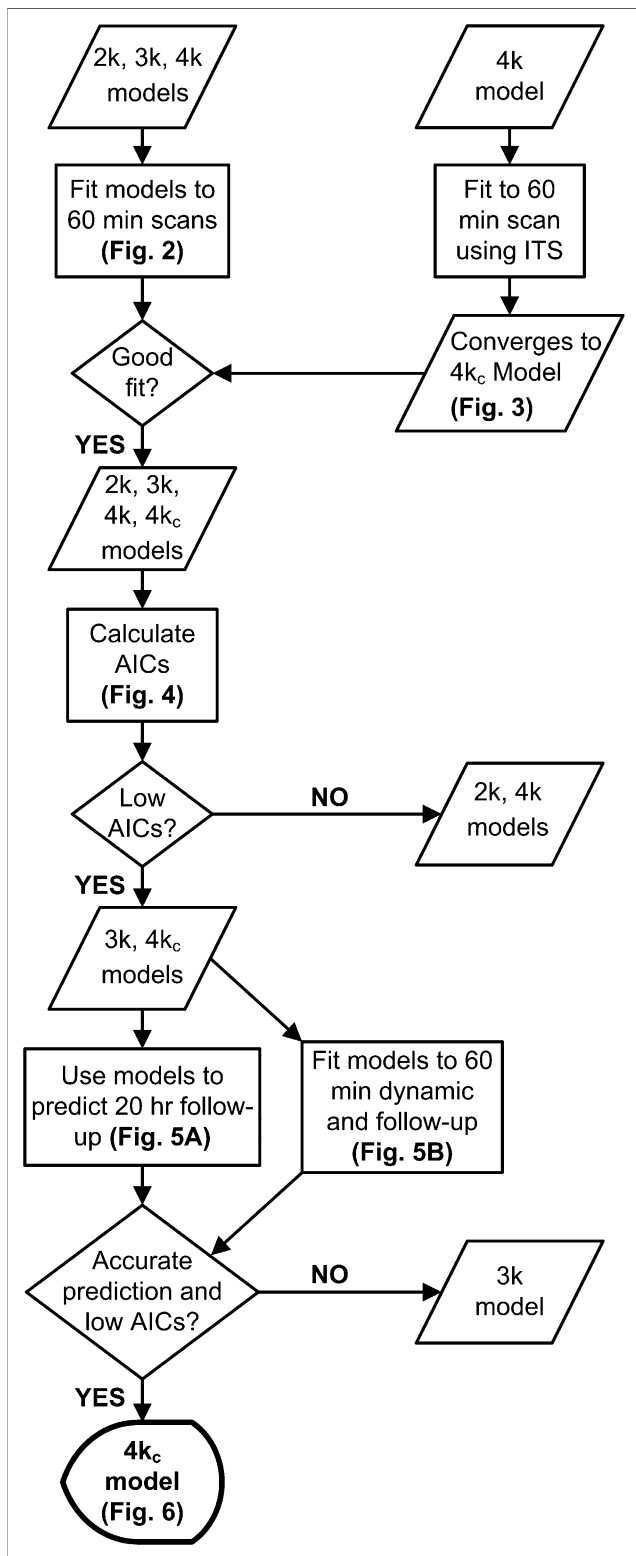


**FIGURE 6.** Model discrimination process by which  $4k_c$  model, compared with 2k, 3k, and 4k models, was determined to be most appropriate for describing *in vivo*  $^{64}\text{Cu}$ -DOTA-RGD kinetics in mouse models that carry  $\alpha_v\beta_3$ -positive tumors.

to rule out the 2k and 4k structures by AIC analysis (Fig. 3) of each model fitted to the initial dynamic PET scans (Fig. 2). The 2k model structure yielded the lowest AICs for tumor time–activity curves in which concentration of free  $\alpha_v\beta_3$  was low (blocked and A431 studies), suggesting that only a single compartment is required to describe  $^{64}\text{Cu}$ -DOTA-RGD kinetics in  $\alpha_v\beta_3$ -negative tissues. Likewise, the 3k and  $4k_c$  models yielded the lowest AICs for tumor time–activity curves in which density of free  $\alpha_v\beta_3$  was high (U373 and U87 studies), suggesting that 2 compartments are needed to describe  $^{64}\text{Cu}$ -DOTA-RGD kinetics in  $\alpha_v\beta_3$ -positive tissues. Implementation of a fixed value of  $k_4$  is supported by the ITS parameter-estimation process, in which  $k_4$  converges to  $0.00938 \text{ min}^{-1}$  for all studies under consideration (Fig. 3), and by graphical analysis, in which Patlak uptake ( $K_i$ ) and Logan volume of distribution ( $V_d$ ) are highly correlated ( $R_S \approx 0.90$ , not shown) across all studies, suggesting little variability in tracer dissociation rate ( $k_4$ ), because  $K_i = f(K_1, k_2, k_3)$  and  $V_d = f(K_1, k_2, k_3, k_4)$  when calculated from fitted model parameters. The 3k model structure is ruled out by fitting 3k and  $4k_c$  models to 60-min dynamic scans plus the 20-h postinjection scan, where the  $4k_c$  structure yields lower AICs (not shown); the 3k model also provides a less accurate prediction of the 20-h postinjection data, compared with 2k, 4k and  $4k_c$  structures (Fig. 4A). Although the PET-derived input function,  $u(t)$ , is corrected for partial-volume effects, errors due to spillover, delay, and dispersion are assumed to be negligible and are not accounted for in the present study. The impact of spillover, in particular, is expected to be small, because uptake of  $\alpha_v\beta_3$ -binding RGD peptides by the myocardium is minimal (4).

By using the 20-h postinjection scans, we were able to estimate  $k_{\text{int}}$ , the rate of irreversible tracer internalization. The black curve in Figure 4B depicts a model fit to selected 20-h data, with the inset showing the first 60 min of data and fit; the gray curve illustrates the effect of setting  $k_{\text{int}}$  to zero, in which a negligible shift from the original fitted black curve is observed (Fig. 4B, inset). The effect of setting  $k_{\text{int}}$  to zero suggests that although the internalization rate is high enough to produce significant retention of the tracer over a 20-h period, the rate does not confound apparent tracer retention because of specific binding to  $\alpha_v\beta_3$  ( $k_3$ ) during the first 60–90 min after tracer injection. Even when fitting the model to data collected over a 20-h period, only a slight decrease in estimated value of  $k_3$  is observed with  $k_{\text{int}}$  included in the model structure, compared with  $k_3$  estimated via a model fit to the 60-min dynamic scan with  $k_{\text{int}}$  set to zero (Fig. 5A). Because tracer metabolite analysis has not yet been performed at 20 h after injection, it is possible that we overestimated  $^{64}\text{Cu}$ -DOTA-RGD plasma concentration at the late static scan. This overestimation would affect the accuracy of the input function past 60 min and thus the confidence level of the estimated value of  $k_{\text{int}}$ . To assess the effect a lower actual tracer plasma concentration 20 h after injection might have on conclusions drawn from the fitted model, we lowered

20-h plasma values calculated from the reconstructed PET image by 2 orders of magnitude and then reestimated the input function as described in the “Parameter Estimation” section. As expected, the resulting  $k_{\text{int}}$  values are higher than those listed in Table 1; however, the fitted model suggests that tracer internalization does not confound the apparent specific binding capacity of the tumor during the first 60 min after tracer injection, even when plasma concentration of tracer at 20 h after injection is assumed to be close to zero. That is, the result is similar to that shown in Figure 4B.

Figure 5A and Table 1 show that the average estimated value of  $k_{\text{int}}$  is much higher in the blocked studies than in the nonblocked studies, suggesting that a greater fraction of  $\alpha_v\beta_3$ -bound peptide may be internalized per unit of time when the 10 mg/kg dose of cold peptide is coinjected with  $^{64}\text{Cu}$ -DOTA-RGD. The  $\alpha_v\beta_3$  integrin is activated by the binding of substrate, which stimulates recycling of the integrin from the cell surface to the intracellular compartment. This process occurs when the integrin binds RGD sequences on molecules such as fibronectin or fibrinogen— analogous to the interaction between the integrin and  $^{64}\text{Cu}$ -DOTA-RGD described by our model—and may explain why internalization rates are higher in tumors exposed to a large bolus of integrin substrate in the form of coinjected cold peptide, compared with tumors exposed to tracer alone. The effect of  $k_{\text{int}}$  on apparent tracer kinetics in blocked studies is similar to the effect seen in nonblocked studies (Fig. 4B).

Estimated values of specific volume of distribution (Table 1) appear to be strongly correlated with concentration of available  $\alpha_v\beta_3$  binding sites within the tumor (Fig. 5B); with the exception of a single A431 study,  $V_S$  increases in parallel with  $\alpha_v\beta_3$  expression from baseline (blocked studies) to low (A431), intermediate (U373), and high (U87) expression. Estimated values of nondisplaceable (nonspecific) tumor uptake are approximately constant, regardless of  $\alpha_v\beta_3$  status (Table 1; Fig. 5B). Along with the AIC analysis presented in Figure 3, which suggests a 1-compartment tissue model is most optimal for describing tracer kinetics in low  $\alpha_v\beta_3$ -expressing tissue, these data support the putative physiologic significance of the 2-compartment tissue model and associated parameters for  $^{64}\text{Cu}$ -DOTA-RGD, in which compartment  $q_1(t)$  represents accumulation of tracer in the tumor resulting from nonspecific transport mechanisms such as extravasation ( $K_1$ ), tissue efflux ( $k_2$ ), and nonspecific binding ( $K_1/k_2$ ). Compartment  $q_2(t)$  represents accumulation in tumor due to specific binding ( $k_3$ ) and dissociation ( $k_4$ ) of tracer from  $\alpha_v\beta_3$ . Additionally, the internalization term  $k_{\text{int}}$  was introduced and is required to fit the model to tracer kinetics measured over a 20-h period (not shown).

Interestingly,  $V_S$  and  $V_{\text{ND}}$  calculated from a previous patient study involving  $^{18}\text{F}$ -galacto-RGD (8) closely match our results. Although variability across patients is not represented here, mean patient  $V_{\text{ND}}$  is virtually identical to  $V_{\text{ND}}$  calculated from our mouse studies and patient  $V_S$  is similar to values calculated for the U373 tumor, which expresses  $\alpha_v\beta_3$  at an intermediate level. This similarity

suggests that the methods and model developed here for kinetic analysis of  $^{64}\text{Cu}$ -DOTA-RGD may be readily applied to patient data.

A high correlation ( $R_S = 0.92$ ) between the ratio of tracer concentration in the tumor at 60 min after injection to tracer concentration in plasma at 10 min  $[C_T(60)]/[C_P(10)]$  and specific volume of distribution ( $V_S$ ) (Fig. 5C) was gleaned from an extensive analysis of correlations between model microparameters ( $V_B, K_1, k_2, k_3, k_4$ ), macroparameters ( $V_S, V_{\text{ND}}, K_i, V_d$ ), and tracer uptake at discrete time points (10, 30, and 60 min). This correlation, along with the aforementioned discussion of patient  $V_S$  and  $V_{\text{ND}}$  values (Fig. 5B), suggests that magnitude of  $\alpha_v\beta_3$  expression could be estimated in a clinical setting on the basis of a blood sample taken at 10 min after injection and a single static PET scan at 60 min.

## CONCLUSION

We conducted a thorough pharmacokinetic analysis of  $^{64}\text{Cu}$ -DOTA-RGD and observed the following. First, we demonstrated that the  $4k_c$  model, compared with the  $2k$ ,  $3k$ , and  $4k$  models, is the most appropriate structure for use with this tracer (and presumably other small molecule tracers that target  $\alpha_v\beta_3$ ) and examined the putative physiologic significance of the 2-compartment tissue model commonly used in PET tracer kinetic analysis by demonstrating that  $V_S$ , calculated on the basis of fitted model parameters, strongly correlates with the concentration of free  $\alpha_v\beta_3$ . Next, we showed that 20-h postinjection scans facilitated quantification of nonspecific internalization of tracer by tumor cells ( $k_{\text{int}}$ ), which is shown to occur at a slow rate relative to specific binding ( $k_3$ ) and dissociation ( $k_4$ ) and, thus,  $k_{\text{int}}$  can be neglected for 1- to 2-h dynamic scans. Third, this model has potential for clinical applications, as demonstrated by the comparison of our results with a previous pharmacokinetic study in patients with cancer, in which the model-based values of  $V_{\text{ND}}$  and  $V_S$  are similar, and the observation that  $V_S$  can be approximated using a single blood sample and static PET scan.

## ACKNOWLEDGMENTS

We thank Dr. David Stout, Dr. Arion Chatzioannou, Waldemar Ladno, and Judy Edwards at the Crump Institute for Molecular Imaging for technical assistance in small-animal imaging; David Truong, David Vu, and Weber Shao (Crump) for computer support; and Stephan Schwarz at the Department of Nuclear Medicine, Medical University of Innsbruck, for excellent technical assistance in producing  $c(\text{RGDFK}(\text{DOTA}))$ . Funding was provided by NCI cancer education grant R25-CA098010.

## REFERENCES

1. Hood JD, Cheresh DA. Role of integrins in cell invasion and migration. *Nat Rev Cancer*. 2002;2:91–100.

2. Shimaoka M, Springer TA. Therapeutic antagonists and conformational regulation of integrin function. *Nat Rev Drug Discov.* 2003;2:703–716.
3. Ruoslahti E. Specialization of tumour vasculature. *Nat Rev Cancer.* 2002;2:83–90.
4. Haubner R, Wester HJ, Weber WA, et al. Noninvasive imaging of  $\alpha_v\beta_3$  integrin expression using  $^{18}\text{F}$ -labeled RGD-containing glycopeptide and positron emission tomography. *Cancer Res.* 2001;61:1781–1785.
5. Haubner R, Weber WA, Beer AJ, et al. Noninvasive visualization of the activated  $\alpha_v\beta_3$  integrin in cancer patients by positron emission tomography and [ $^{18}\text{F}$ ]galacto-RGD. *PLoS Med.* 2005;2:e70.
6. Beer AJ, Haubner R, Sarbia M, et al. Positron emission tomography using [ $^{18}\text{F}$ ]galacto-RGD identifies the level of integrin  $\alpha_v\beta_3$  expression in man. *Clin Cancer Res.* 2006;12:3942–3949.
7. Beer AJ, Lorenzen S, Metz S, et al. Comparison of integrin  $\alpha_v\beta_3$  expression and glucose metabolism in primary and metastatic lesions in cancer patients: a PET study using  $^{18}\text{F}$ -galacto-RGD and  $^{18}\text{F}$ -FDG. *J Nucl Med.* 2008;49:22–29.
8. Beer AJ, Haubner R, Goebel M, et al. Biodistribution and pharmacokinetics of the  $\alpha_v\beta_3$ -selective tracer  $^{18}\text{F}$ -galacto-RGD in cancer patients. *J Nucl Med.* 2005;46:1333–1341.
9. Akaike H. A new look at the statistical model identification. *IEEE Trans Automat Contr.* 1974;AC-19:716–723.
10. Bertoldo A, Sparacino G, Cobelli C. “Population” approach improves parameter estimation of kinetic models from dynamic PET data. *IEEE Trans Med Imaging.* 2004;23:297–306.
11. Balasubramanian S, Kuppaswamy D. RGD-containing peptides activate S6K1 through  $\beta_3$  integrin in adult cardiac muscle cells. *J Biol Chem.* 2003;278:42214–42224.
12. Roberts MS, Woods AJ, Dale TC, Van Der Sluijs P, Norman JC. Protein kinase B/Akt acts via glycogen synthase kinase 3 to regulate recycling of  $\alpha_v\beta_3$  and  $\alpha_5\beta_1$  integrins. *Mol Cell Biol.* 2004;24:1505–1515.
13. Decristoforo C, Hernandez Gonzalez I, Carlsen J, et al.  $^{68}\text{Ga}$ - and  $^{111}\text{In}$ -labelled DOTA-RGD peptides for imaging of  $\alpha_v\beta_3$  integrin expression. *European J Nucl Med Mol Imaging.* 2008; 35:1507–1515.
14. Wu Y, Zhang X, Xiong Z, et al. microPET imaging of glioma integrin  $\alpha_v\beta_3$  expression using  $^{64}\text{Cu}$ -labeled tetrameric RGD peptide. *J Nucl Med.* 2005; 46:1707–1718.
15. Tai YC, Ruangma A, Rowland D, et al. Performance evaluation of the microPET focus: a third-generation microPET scanner dedicated to animal imaging. *J Nucl Med.* 2005;46:455–463.
16. Su H, Bodenstern C, Dumont RA, et al. Monitoring tumor glucose utilization by positron emission tomography for the prediction of treatment response to epidermal growth factor receptor kinase inhibitors. *Clin Cancer Res.* 2006; 12:5659–5667.
17. Loening AM, Gambhir SS. AMIDE: a free software tool for multimodality medical image analysis. *Mol Imaging.* 2003;2:131–137.
18. Ferl GZ, Zhang X, Wu HM, Huang SC. Estimation of the  $^{18}\text{F}$ -FDG input function in mice by use of dynamic small-animal PET and minimal blood sample data. *J Nucl Med.* 2007;48:2037–2045.
19. Nakamura Y, Tsuji M, Arai S, Ishihara C. A method for rapid and complete substitution of the circulating erythrocytes in SCID mice with bovine erythrocytes and use of the substituted mice for bovine hemoprotozoa infections. *J Immunol Methods.* 1995;188:247–254.
20. Castel S, Pagan R, Mitjans F, et al. RGD peptides and monoclonal antibodies, antagonists of  $\alpha_v$ -integrin, enter the cells by independent endocytic pathways. *Lab Invest.* 2001;81:1615–1626.
21. SAAM II v1.2/PopKinetics v1.0, version Windows. Seattle, WA: SAAM Institute. Available at: <http://depts.washington.edu/saam2/software.html>. Accessed January 6, 2009.
22. Barrett PH, Bell BM, Cobelli C, et al. SAAM II: simulation, analysis, and modeling software for tracer and pharmacokinetic studies. *Metabolism.* 1998; 47:484–492.
23. Callegari T, Caumo A, Cobelli C. Generalization of map estimation in SAAM II: validation against ADAPT II in a glucose model case study. *Ann Biomed Eng.* 2002;30:961–968.
24. Innis RB, Cunningham VJ, Delforge J, et al. Consensus nomenclature for in vivo imaging of reversibly binding radioligands. *J Cereb Blood Flow Metab.* 2007; 27:1533–1539.
25. Patlak CS, Blasberg RG, Fenstermacher JD. Graphical evaluation of blood-to-brain transfer constants from multiple-time uptake data. *J Cereb Blood Flow Metab.* 1983;3:1–7.
26. Stedman TL. *Stedman’s Medical Dictionary.* 27th ed. Philadelphia, PA: Lippincott Williams & Wilkins; 1999.